Inorganic Chemistry

Article

pubs.acs.org/IC

Pteridine Cleavage Facilitates DNA Photocleavage by Ru(II) Polypyridyl Compounds

Benjamin R. Williams,[†] Shannon R. Dalton,[†] Meredith Skiba,[†] Sung Eun Kim,[†] Allison Shatz,[†] Patrick J. Carroll,[‡] and Sharon J. Nieter Burgmayer*[,†]

[†]Department of Chemistry, Bryn Mawr College, Bryn Mawr, Pennsylvania 19010, United States

[‡]Department of Chemistry, University of Pennsylvania, Philadelphia, Pennsylvania 19104, United States

Supporting Information

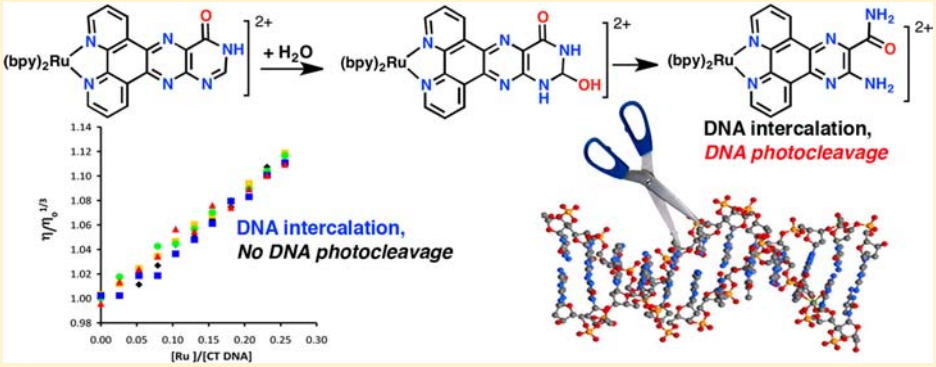

ABSTRACT: The synthesis, characterization, binding to calf thymus DNA, and plasmid DNA photocleavage studies of two ruthenium(II) pteridinylphenanthroline complexes are reported where the new pteridinylphenantholine ligands in these complexes are additions to a larger family designed to resemble DNA bases. $[Ru(bpy)_2(L\text{-keto})](PF_6)_2$ **1** is synthesized from ligand substitution of $Ru(bpy)_2Cl_2$ by 4-keto-pteridino[6,7-*f*]phenanthroline (L-keto). Increasing the reaction temperature during synthesis of **1** causes a ring scission of the L-keto ligand within the pyrimidine ring yielding a second Ru complex, $[Ru(bpy)_2(L\text{-aap})](PF_6)_2$ **2** where L-aap is 2-amino-3-amidopyrazino[5,6-*f*]phenanthroline. The ring cleavage reaction is accompanied by the loss of one carbon in the pyrimidine ring. Complexes **1** and **2** are characterized by ^{1}H NMR, UV/visible absorption and FT-IR spectroscopies and by cyclic voltammetry, and these results are presented in comparison to the previously reported related complexes $[Ru(bpy)_2(L\text{-allox})](PF_6)_2$, $[Ru(bpy)_2(L\text{-amino})](PF_6)_2$, and $[Ru(bpy)_2(dppz)](PF_6)_2$. In addition, **2** has been structurally characterized by X-ray diffraction. Both **1** and **2** are good intercalators of calf thymus DNA as determined by viscometry and binding constants obtained from absorption titrations. Only the ring-cleaved complex **2** exhibits a high degree of pBR322 plasmid photocleavage in contrast to the other pteridinyl-phenanthroline complexes, which exhibit no plasmid DNA photocleavage. Complex **1**, however, decomposes in buffer forming the photocleaver **2**, demonstrating that sample age and reactivity can affect observed photocleavage. Complex **2** appears to photocleave DNA through a singlet oxygen mechanism.

INTRODUCTION

Transition metal complexes are highly useful probes of biological macromolecular behavior, as shown through a wide variety of studies on transition metal complexes interacting with DNA.[1−4] Because of their photophysical and redox properties, metal complexes have the capacity to cause DNA damage by photoinduced oxidative strand breakage[5,6] and to mediate charge transport through DNA.[7,8] Intercalative binding by metal complexes can disrupt the helical nature of DNA, causing profound effects on DNA integrity and cell viability.[9] For these reasons, investigations of DNA interactions with transition metal complexes continues to be a vibrant area of research for potential anticancer pharmaceuticals, diagnostics, signaling, and theraputic applications.[10,11]

One subset of inorganic photocleavage agents is the polypyridylruthenium intercalators. Octahedral ruthenium(II) complexes with ligands derived from 1,10-phenanthroline such as dipyridophenazine (dppz) are established intercalative compounds and some have the ability to photooxidize DNA.[3,12] In particular, $[Ru(N{-}N)_2(dppz)]^{2+}$ (where N−N is 2,2′-bipyridine or 1,10-phenanthroline) has been widely studied because of its unique "molecular light switch" properties and strong intercalative binding to DNA (Figure 1A).[13−15] As a result, $[Ru(N{-}N)_2(dppz)]^{2+}$ has been a prototype for the development of other derivatives where structural variation of the intercalating ligand (e.g., dppz) as well as varying the ancillary ligand sets (i.e., the N−N ligands) has been studied with respect to DNA photocleavage. A selection of complexes is shown in Figure 1 to illustrate the variety of planar conjugated

Received: June 7, 2012
Published: November 20, 2012

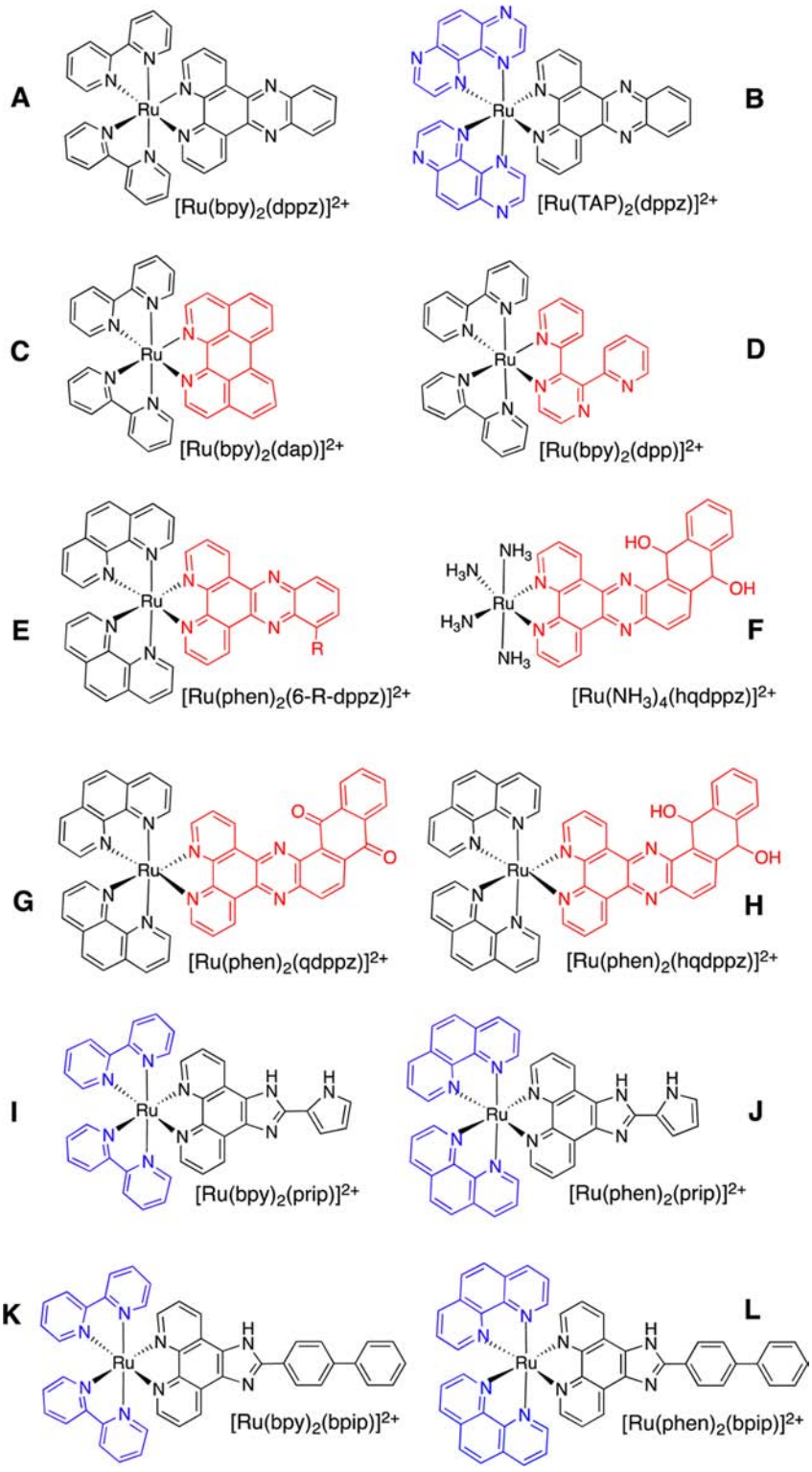

Figure 1. Structures of photocleaving ruthenium(II) polypyridyl complexes mentioned in the text. The variation in the intercalating ligand is highlighted in red while variation of ancillary ligands in several studies is highlighted in blue.

π systems built into the intercalating ligand. Photocleaving agents are almost always characterized as intercalating compounds; however, not all compounds that bind DNA in this manner possess photocleaving properties. For instance, all complexes in Figure 1 intercalate DNA,[16−23] but only complex F fails to photocleave plasmid DNA.[20] The redox level of the intercalating ligand can also impact photocleavage efficiency, as was observed in the higher level of photocleavage by the oxidized quinone in G compared to the reduced hydroquinone in H.[21] The role that the ancillary ligand plays in binding and DNA cleavage has been investigated. Two studies[22,23] comparing the relative photocleavage ability of *bis*(bipyridine) versus *bis*(phenanthroline) ancillary ligand sets in I, J, K, and L have reported the same results: complexes of phenanthroline

dx.doi.org/10.1021/ic301219z | *Inorg. Chem.* 2012, 51, 12669−12681

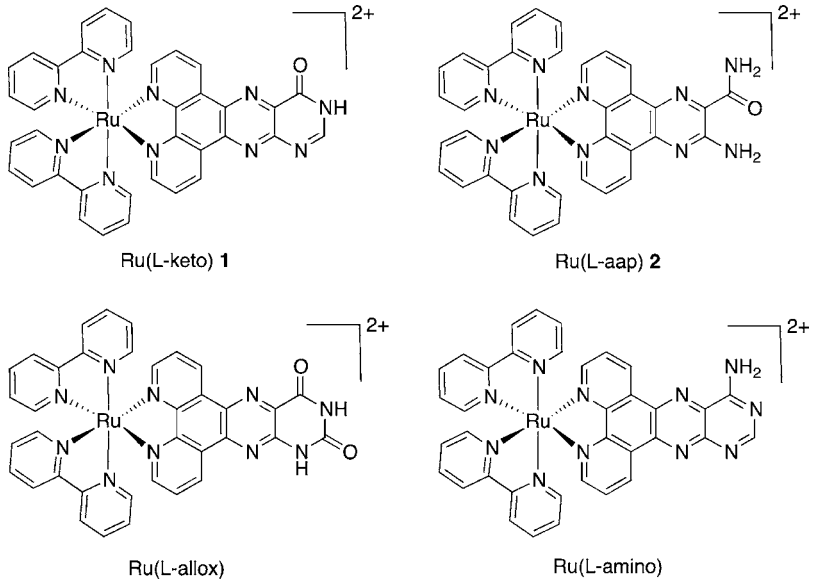

Figure 2. Four Ru complexes discussed in this study, all isolated as hexafluorophosphate salts.

exhibit greater plasmid DNA photocleavage than bipyridine complexes possessing the same intercalating ligand. A recent X-ray crystal structure showing for the first time a DNA-bound Ru-polypyridyl complex provides structural evidence for how the ancillary ligand may participate in the DNA binding that precedes an oxidative cleavage event.[24] In this structure, complex B (Figure 1) exhibits two simultaneous binding modes to duplex DNA. Its dppz ligand interacts by intercalation as expected, while one of the tetraazaphenanthrene (TAP) ligands binds by a partial or semi-intercalation into an adjacent duplex strand causing substantial DNA duplex kinking.

We previously reported the synthesis of a family of five ruthenium(II) pteridinylphenanthroline complexes that intercalate calf thymus DNA (CT DNA) with binding constants similar to that of $[Ru(bpy)_2(dppz)]^{2+}$.[25] This family was designed to incorporate new polypyridine ligands whose pteridine and pterin units structurally resemble DNA bases. In this work, that family has been expanded to include two new complexes, $[Ru(bpy)_2(L\text{-keto})]^{2+}$ **1** and $[Ru(bpy)_2(L\text{-aap})]^{2+}$ **2** where complex **2** is derived from **1** via a pyrimidine ring-cleavage reaction. Here we report the synthesis and characterization, DNA-binding, and photocleavage studies of **1** and **2** together with related complexes Ru(L-allox) and Ru(L-amino) for comparison (Figure 2). Remarkably, only the ring-cleaved complex **2** exhibits a high degree of pBR322 plasmid photocleavage, in contrast to the pteridine complexes that uniformly exhibit no plasmid DNA photocleavage. In addition we show that **1** spontaneously degrades in buffer to form **2**, an example of in situ reactivity of a Ru complex under photocleavage experiment conditions that can result in misleading photocleavage behavior.

EXPERIMENTAL SECTION

Materials and Methods. The synthesis of 1,10-phenanthroline-5,6-dione followed the procedure of Yamada et al.[26] *cis*-Dichloro-*bis*(bipyridyl)ruthenium(II) dihydrate was synthesized using the procedure according to Sullivan et al.[27] The preparation of $[Ru(bpy)_2(L\text{-amino})](PF_6)_2$ and $[Ru(bpy)_2(L\text{-allox})](PF_6)_2$ followed a published procedure.[25] All other reagents were purchased from Sigma-Aldrich. High resolution ESI-MS (HRESI-MS) were obtained at the Mass Spectrometry Facility in the Department of Chemistry at the University of Arizona on an Ion Spec Fourier Transform Mass Spectrometer or from a Waters Micromass-ZQ mass spectrometer at Bryn Mawr College by infusion of samples as acetonitrile solutions. ^{1}H NMR spectra, both as 1D and 2D experiments were obtained using a Bruker 400 MHz FT-NMR spectrometer. Infrared spectra were obtained from a Perkin-Elmer Spectrum 2000 FT-IR on samples prepared as KBr pellets. FT-IR spectra intensities are qualitatively indicated as vs = very strong, s = strong, m = medium, w = weak. Electronic absorption spectra were produced using quartz cuvettes with a Beckman-Coulter DU 800 spectrophotometer analyzing 30 μM solutions of **1**, **2**, and other complexes in 10 mM sodium phosphate buffer (pH 7). Cyclic voltammetry (CV) was performed on a BAS CV-50W using 0.10 M tetrabutylammonium perchlorate (TBAP) as electrolyte in acetonitrile with a Ag wire reference electrode and a Pt working electrode. Potentials are referenced to the internal standard ferrocenium/ferrocene (Fc^+/Fc), which occurs at +0.400 V vs a Ag/AgCl reference electrode.

Syntheses. *4-Ketopteridino(6,7-f)phenanthroline (L-keto).* A solution of 4,5-diamino-6-hydroxypyrimidine hemisulfate (0.3503 g, 1 mmol) in 20 mL of water was prepared adding 3 M NaOH dropwise to pH 10. This was added to a solution of 1,10-phenanthroline-5,6-dione (0.2101 g, 1 mmol) in 20 mL of methanol. The resulting dark-brown mixture was allowed to stir at room temperature for approximately 20 h. The cream-colored precipitate was isolated via vacuum filtration, washed using approximately 5 mL each of cold water, cold methanol, and room temperature diethyl ether, and was subsequently dried under vacuum. Yield 0.2740 g (91%). IR (KBr, cm^{-1}): 1705s, 1636s, 1607s, 1538m, 1452m, 1408m, 1370s cm^{-1}. ^{1}H NMR (10% CF_3CO_2D in $CDCl_3$, δ/ppm): 8.36 (t, 1H), 8.42 (t, 1H), 9.42 (m, 3H), 9.91 (d, 1H), 10.20 (d, 1H). Anal. Calcd (%) for $C_{16}H_8N_6O{\cdot}0.5\ H_2O$: C, 62.14; H, 2.93; N, 27.17. Found: C, 62.44; H, 2.47; N, 27.43.

$[Ru(bpy)_2(L\text{-keto})](PF_6)_2$ ***1.*** L-keto (0.2250 g, 0.7 mmol) and $Ru(bpy)_2Cl_2$ (0.3625 g, 0.7 mmol) were combined in 20 mL of ethylene glycol and 5 mL of water and deaerated by bubbling with nitrogen gas. The dark purple mixture was heated under a nitrogen atmosphere for 3 h at 110 °C with stirring. The mixture was then cooled to room temperature, diluted with 20 mL of water, and vacuum filtered to remove any insoluble material. The product was precipitated as a hexafluorophosphate salt by adding NH_4PF_6 solution in excess (~0.6 g). The suspension was vacuum filtered and subsequently washed with approximately 5 mL each of cold water, cold ethanol, and room temperature diethyl ether. The resulting light orange solid was dried under vacuum and purified by chromatography on neutral alumina using 1:1 acetonitrile-methanol eluent (v/v). Yield 0.2785 g

dx.doi.org/10.1021/ic301219z | *Inorg. Chem.* 2012, 51, 12669−12681

(37%). IR (KBr, cm^{-1}): 1716s, 1606s, 1546m, 1466m, 1447m, 1419m, 1387m, 1366, 841vs, 763m, 558s cm^{-1}. ^1H NMR (DMSO-d_6, δ/ppm): 13.28 (s, 1H), 9.51 (d, 1H), 9.45 (d, 1H), 8.89 (m, 4H), 8.61 (s, 1H), 8.30 (d, 1H), 8.22 (m, 3H), 8.13 (t, 2H), 8.02 (m, 2H), 7.82 (d, 2H), 7.75 (t, 2H), 7.61 (t, 2H), 7.39 (t, 2H). Anal. Calcd. (%) for $C_{36}H_{24}F_{12}N_{10}OP_2Ru{\cdot}3H_2O$: C, 40.88; H, 2.86; N, 13.24. Found: C, 40.23; H, 2.54; N, 12.92. MS (HRESI) m/z 357.0590 (calcd for $[M]^{2+}$ 357.0588, M = $C_{36}H_{24}N_{10}ORu$).

[Ru(bpy)$_2$(L-aap)](PF$_6$)$_2$ **2**. L-keto ligand (0.1030 g, 0.3 mmol) and $Ru(bpy)_2Cl_2$ (0.1660 g, 0.3 mmol) were combined in 10 mL of ethylene glycol and 4 mL of water and deaerated. The dark purple mixture was heated under nitrogen gas for 3 h at 110 ± 2 °C. The temperature was increased to 140 ± 3 °C from 110 °C over 15 min and heated for another 2.5 h. The mixture was cooled to room temperature, diluted with 20 mL of water, and then vacuum filtered. Excess NH_4PF_6 (0.6 g) was added to the dark red filtrate to produce a light orange suspension. This was vacuum filtered and subsequently washed with approximately 5 mL each of cold water, cold ethanol, and room temperature diethyl ether. The resulting light orange solid was dried under vacuum and then chromatographed with neutral alumina using acetonitrile eluent. Yield 0.1062 g (35%). IR (KBr, cm^{-1}): 1683s, 1591s, 1465m, 1447m, 1423m, 1380m, 1307w, 1184w, 841vs, 762m, 730s, 558s cm^{-1}. ^1H NMR (DMSO-d_6, ppm): δ 7.37 (t, 2H), 7.57 (t, 2H), 7.67 (t, 2H), 7.82 (d, 2H), 7.84–8.00 (m, 3H), 8.13 (t, 2H), 8.22 (m, 5H), 8.86 (t, 4H), 9.04 (s, 1H), 9.25 (dd, 1H), 9.79 (dd, 1H); (acetone-d_6, δ/ppm): 7.33 (s, 1H), 7.41 (m, 2H), 7.64 (m, 2H), 7.92 (m, 1H), 8.00 (m, 3H), 8.16 (m, 4H), 8.26 (m, 2H), 8.33 (dd, 1H), 8.50 (dd, 1H), 8.73 (s, 1H), 8.82 (m, 4H), 8.92 (s, 1H), 9.39 (dd, 1H), 9.68 (dd, 1H). Anal. Calcd. (%) for $C_{35}H_{26}F_{12}N_{10}OP_2Ru{\cdot}2H_2O$: C, 40.83; H, 2.94; N, 13.60. Found: C, 40.72; H, 2.87; N, 13.37. MS (HRESI) m/z 352.0671, (calcd for $[M]^{2+}$ 352.0666, M = $C_{35}H_{26}N_{10}ORu$); $[M+(PF_6)]^+$ 849.1256.

X-ray Crystallography. Suitable crystals of **2** were formed by vapor-diffusion of chloroform into acetonitrile solutions of **2** producing orange trigonal pyramidal-shaped crystals. X-ray diffraction experiments were performed at the University of Pennsylvania in Philadelphia, Pennsylvania. $C_{73}H_{56}P_4N_{21}O_2F_{24}Cl_3Ru_2$ crystallizes in the triclinic space group $P\bar{1}$ with a = 12.5301(9) Å, b = 17.2969(11) Å, c = 21.1287 Å, α = 99.010(3)°, β = 106.559(2)°, γ = 103.733(2)°, V = 4138.3(5) Å^3, Z = 2, and d_{calc} = 1.724 g/cm^3. X-ray intensity data were collected on a Bruker APEXII CCD area detector employing graphite-monochromated Mo–Kα radiation (λ = 0.71073 Å) at a temperature of 143(1) K. Preliminary indexing was performed from a series of thirty-six 0.5° rotation frames with exposures of 20 s. A total of 3,384 frames were collected with a crystal to detector distance of 37.600 mm, rotation widths of 0.5°, and exposures of 20 s: A total of 125,441 reflections were measured over the ranges $1.73 \le \theta \le 27.67°$, $-16 \le h \le 16$, $-19 \le k \le 22$, $-27 \le l \le 27$ yielding 18,809 unique reflections (R_{int} = 0.0291). The intensity data were corrected for Lorentz and polarization effects and for absorption using SADABS (minimum and maximum transmission 0.6634, 0.7456).[28] Data were processed, and the structure was solved by direct methods using (SHELXS-97).[29] Additional details are available in the Supporting Information.

DNA Studies. All buffer solutions were prepared in sterile, deionized water. Ru solutions for viscosity titrations were prepared in acetonitrile. Double-stranded calf thymus (CT DNA) was purchased from Sigma-Aldrich. Solutions of DNA used for viscometry were made with 10 mM sodium phosphate buffer (pH 7) with 50 mM NaCl. In a typical preparation, CT DNA (Type 1 fibers) was added to a 10 mM phosphate buffer (pH 7) and 50 mM NaCl, and sonicated for approximately 2 h. The solution was vortexed, centrifuged for 12 min, and the supernatant isolated from any particulate matter pelleted during centrifugation. DNA concentrations were determined by absorption spectroscopy employing the following extinction coefficients at 260 nm: CT DNA: 6,600 M^{-1} cm^{-1} (per nucleotide), 13,100 M^{-1} cm^{-1} (per base pair).[30] Solutions of pBR322 DNA (New England BioLabs) were prepared by diluting the stock plasmid with a 50 mM Tris-HCl (pH 7.2) and 18 mM NaCl buffer. Ruthenium solutions for photocleavage experiments were also prepared in 50 mM Tris-HCl (pH 7.2) and 18 mM NaCl buffer. Ruthenium solutions were stored in the dark to prevent photodegredation. For positive controls in photocleavage experiments, pBR322 plasmid was nicked using Nb.BsmI (New England BioLabs).

Viscometry. An Ostwald viscometer in a noncirculating water bath at 22–23 °C was used to measure the relative viscosity of DNA solutions in the presence of Ru complexes. The concentrations of the Ru complex and CT DNA were chosen to minimize the volume of Ru complex added to a solution of DNA concentrated enough to make changes in the slope maximally distinguishable. A 2.5 mM stock solution of each Ru complex was prepared in acetonitrile because of its limited solubility in aqueous buffer. A 0.30 mM (per bp) solution of CT DNA was titrated with Ru complex over the range 0–0.2 [Ru]/[DNA]. Upon each addition of Ru complex, the solution in the viscometer was bubbled with nitrogen gas to aid mixing. The solution was then drawn up through the capillary portion of the viscometer using a pipet bulb, and a stopwatch was used to time the downward flow of the solution. In accordance with the theory of Cohen and Eisenberg,[31] the resulting data were plotted as intrinsic viscosity, $(\eta/\eta_o)^{1/3}$ versus the ratio of complex to DNA. The ratio $(\eta/\eta_o)^{1/3}$ was calculated based on eq 1, where η is the viscosity of DNA in the presence of the complex, t_f is the flow time of the experimental trial in seconds, t_o is the flow time of buffer in seconds, and η_o is the viscosity of DNA solution in the absence of complex.

$$\eta = \frac{t_f - t_o}{t_o} \quad (1)$$

Photocleavage. Experiments were carried out using 0.1 μg of supercoiled pBR322 in a sample volume of 15 μL. Plasmid DNA pBR322 was treated with desired [Ru]. The samples were irradiated at room temperature with a UV lamp (365 nm, 8 W). Samples were analyzed by electrophoresis for 1.5 h at 80 V on a 1% agarose gel containing 0.5 μg/mL ethidium bromide. A Bio-Rad Molecular Imager Gel Doc XR+ was used to visualize the gels by UV illumination. Reactive oxygen species (ROS) experiments used sodium azide and DMSO solutions prepared in 50 mM Tris-HCl (pH 7.2) and 18 mM NaCl buffer. Bovine SOD (Sigma-Aldrich) was dissolved in 10 mM phosphate buffer pH 7.5 at 1 unit/μL. These solutions were added into the plasmid DNA and ruthenium sample and irradiated. To run the experiment under anaerobic conditions all solutions were thoroughly bubbled with nitrogen and brought into a glovebag filled with a nitrogen atmosphere. The samples were prepared and irradiated within the glovebag.

Isothermal Binding Titrations. The absorption titrations were performed at room temperature using a constant concentration of ruthenium complex in each sample, with an increasing concentration of CT DNA. The samples were prepared using 10 mM phosphate buffer (pH 7) with 50 mM NaCl. The concentrations of metal compounds were between 12.5 and 23 μM depending on extinction coefficient of individual compound, and CT DNA was added until the [DNA]/[Ru] ratio was in the range 6–9, depending on compound. Samples were incubated at room temperature for 10 min before absorption spectra were recorded. The binding constant K and the site size, s, were extracted from the absorption data fitted to eqs 2 and 3:[32]

$$(\varepsilon_a - \varepsilon_f)/(\varepsilon_b - \varepsilon_f) = [b - (b^2 - 2K^2C[\mathrm{DNA}]/s)]^{1/2}/2KC \quad (2)$$

$$b = 1 + KC + K[\mathrm{DNA}]/2s \quad (3)$$

where C is the constant total concentration of Ru species, [DNA] is the total concentration of added DNA as M base pairs, ε_a is the apparent absorption in the presence of DNA, ε_f is the extinction coefficient of free Ru complex in the buffer, and ε_b is the extinction coefficient of the DNA-bound Ru complex. The value of ε_f was obtained from a Beer's plot of the Ru complex while the value of ε_b was obtained from the absorbance of a saturated Ru-DNA sample divided by the concentration C.

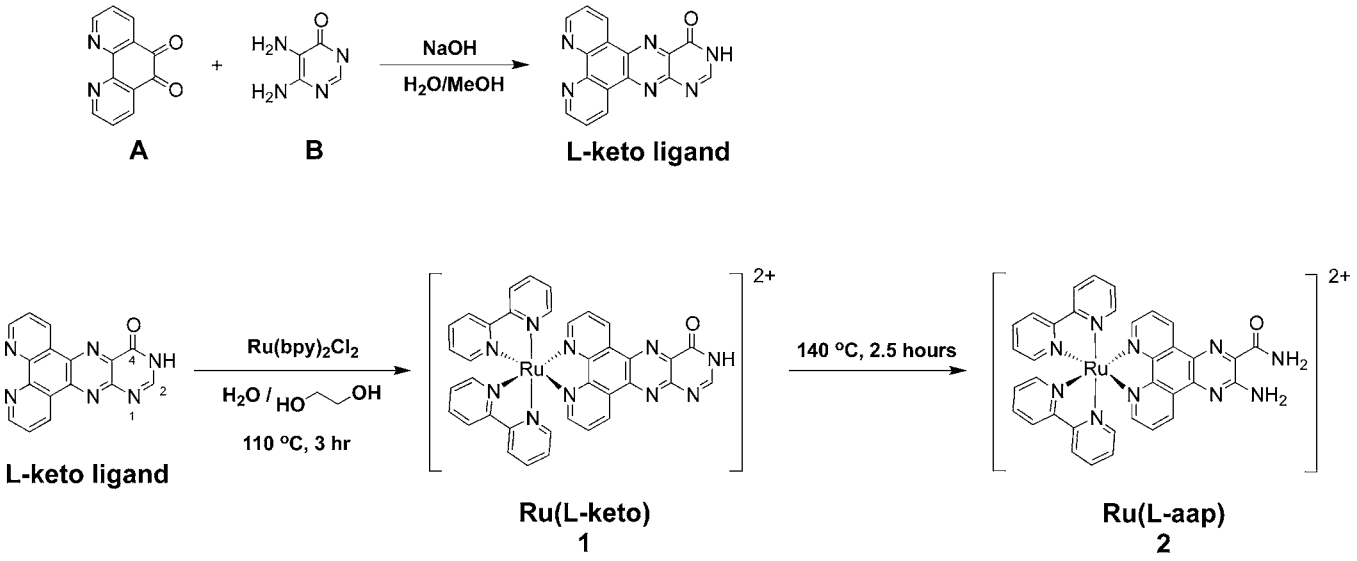

Figure 3. Synthetic pathway for the formation of L-keto ligand and $[Ru(L\text{-}aap)]^{2+}$. Both $[Ru(L\text{-}keto)]^{2+}$ and $[Ru(L\text{-}aap)]^{2+}$ complexes are isolated as the PF_6^- salts.

RESULTS AND DISCUSSION

Syntheses. We describe here two new compounds in the family of *bis*(bipyridine)Ru(II) complexes chelated by pteridinyl-phenanthroline ligands. Both compounds are derived from the bidentate ligand 4-ketopteridino(6,7-*f*)phenanthroline (L-keto) that is formed from the condensation reaction of 1,10-phenanthroline-5,6-dione and 4,5-diamino-6-hydroxypyrimidine. L-keto reacts with $Ru(bpy)_2Cl_2$ heated in ethylene glycol and water (110 °C, 3 h) forming the complex $[Ru(bpy)_2(L\text{-}keto)]^{2+}$, which is isolated as the bright orange hexafluorophosphate salt $[Ru(bpy)_2(L\text{-}keto)](PF_6)_2$ **1** upon the addition of excess ammonium hexafluorophosphate. Further purification of **1** by chromatography on alumina is required to separate **1** from unreacted $Ru(bpy)_2Cl_2$ and byproduct **2**, described below.

Pteridine Ring Cleavage Reaction. During the synthesis of **1**, when the reaction temperature is increased above 120 °C, a second reaction occurs at the coordinated L-keto ligand producing an unexpected byproduct. The pyrimidine ring of Ru(II)-coordinated L-keto is cleaved with excision of the −CH group at position 2 to yield an amino, amido-substituted pyrazinophenanthroline complex $[Ru(bpy)_2(L\text{-}aap)](PF_6)_2$ **2** (Figure 3). Direct synthesis of **2** is best accomplished via a two-step process where L-keto is first chelated to $Ru(bpy)_2^{2+}$ by thermal ligand substitution of $Ru(bpy)_2Cl_2$ at 110 °C, followed by increasing the reaction temperature to 140 °C to complete the pteridine ligand ring-opening reaction.

The pyrimidine ring cleavage reaction occurs at the unsubstituted C atom in the pyrimidine ring. This site has increased electrophilicity resulting from the electronic effect of the two neighboring electronegative nitrogen atoms N1 and N3. Alkaline conditions have previously been reported to cause ring cleavage in pteridines and other pyrimidine-containing compounds. The literature suggests this involves hydration across the N1−C2 bond to initiate the ring-opening event followed by a second attack by hydroxide at C2 hydroxide causing C2 to be excised from the ring by deformylation.[33−39] In the work reported here, pteridine cleavage in complex **1** to form **2** is accomplished at high temperature in the presence of water, where water provides hydroxide for the ring-opening event, possibly through Ru(L-keto) acting as a weak base. Consistent with the proposed mechanism, the addition of 2 equiv of aqueous NaOH to **1** accelerates pteridine ring-opening, forming complex **2** within 30 min. Unfortunately, base addition also produces a dimeric Ru side-product as detected by ESI-MS in addition to **2**. For this reason, the preferred synthetic method to **2** relies on elevated temperatures only, without addition of NaOH.

Chelation of L-keto to Ru(II) appears to facilitate pyrimidine cleavage. Attempts to accomplish an analogous ring cleavage in the uncoordinated, free L-keto ligand using only heat produced no ring-opened product after 6 h reflux in a 40% ethanol/water solution. Addition of 2 equiv of NaOH to the refluxing ligand in aqueous ethanol produced 31% conversion to ring-opened product within 3 h. These results can be compared to the ring-cleavage reaction of Ru(L-keto) **1**, where conversion to the ring-opened product **2** occurs within 3 h at 140 °C and within 30 min using 2 equiv of NaOH at 110 °C. The more facile ring cleavage of **1** as compared to the uncoordinated ligand could be due to the electron withdrawing nature of the Ru(II) metal as a Lewis acid increasing the electrophilicity of atom C2, or an electrostatic effect where the dicationic charge of the complex favors interaction with an anionic nucleophile like hydroxide.

Characterization. The ruthenium complexes **1** and **2** were characterized using ESI-MS and HRESI-MS, ^1H NMR, COSY and NOESY NMR, FT-IR spectroscopy, electronic spectroscopy, and CV. Complex **2** was structurally characterized by single crystal X-ray diffraction.

ESI-MS. ESI-MS was especially useful to monitor the reactions leading to **1** and **2** for optimizing the synthetic procedure. ESI-MS spectra show the **1** and **2** dications $[M]^{2+}$ at m/z 357 and 352, respectively, as the major species in addition to the PF_6 adducts $[M+PF_6]^+$ at 859 and 849 m/z. All signals showed the expected ruthenium isotope pattern where a compressed pattern was observed for the dication consistent with its 2+ charge.

Figure 4 shows the relative abundance of **1** (red line) and **2** (green line) as well as starting material $Ru(bpy)_2Cl_2$ (blue line, detected as the cation $[Ru(bpy)_2Cl(acetonitrile)]^+$ at m/z 490) as a function of time to illustrate the reaction progress. The reaction is held at 110 °C for the first 4 h and during this period

dx.doi.org/10.1021/ic301219z | *Inorg. Chem.* 2012, 51, 12669−12681

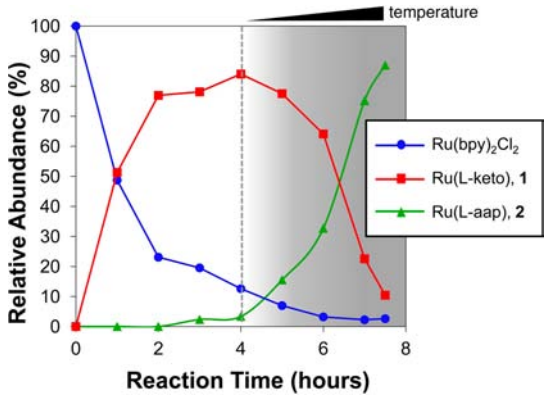

Figure 4. Percent abundance of $Ru(bpy)_2Cl_2$ Ru(L-keto) **1** and Ru(L-aap) **2** determined by mass spectrometry over the course of the reaction. The reaction temperature was increased from 110 to 140 °C as indicated by the black wedge in the top right corner.

$[Ru(bpy)_2Cl(acetonitrile)]^+$ disappears because of the complexation of L-keto ligand with the $[Ru(bpy)_2]^{2+}$, forming **1**. While a small amount of ring-cleaved product **2** forms after about 2 h, the conversion of **1** to **2** is accelerated by increasing the reaction temperature to 140 °C. Figure 3 shows that 4 h after the temperature was increased from 110 to 140 °C, the rapid appearance of **2** parallels the sudden decrease in **1** abundance between hours 6 and 7, indicating that complex **2** is indeed produced at the detriment of **1**.

X-ray Crystal Structure of [Ru(bpy)$_2$(L-aap)](PF$_6$)$_2$ 2. Complex **2** is easily crystallized from several solvent environments. Microcrystalline **2** was produced by evaporation of acetonitrile solutions whereas larger single crystals suitable for X-ray analysis formed as long rectangular parallelpipeds from acetonitrile/water, acetone/water and acetone/alcohol mixtures. Crystals grown under these conditions exhibited good form as evaluated by microscopy, but X-ray diffraction consistently showed badly disordered hexafluorophosphate counterions and disorder in the L-aap ligand, which limited structure solution refinement. To eliminate this disorder problem, PF_6^- anion exchange with perchlorate, triflate, tetraphenylborate, and *d*-tartrate anions was performed. Though the anion exchange was successful and produced single crystals, these also contained disordered anions and/or disorder within the L-aap ligand positions. Ultimately the solvent mixture acetonitrile/chloroform produced crystals of **2** $(PF_6)_2$ having a distinctly different morphology that permitted a reasonable structure solution refinement to $R = 9\%$ where only one of the PF_6^- ions persisted as disordered. One of the PF_6^- ions (P3, F13–F18) was disordered by displacement of the phosphorus atom by about 0.5 Å, and this anion was modeled by two PF_6^- groups; bond distance restraints were applied, and the fluorine atoms were assigned constant isotropic thermal parameters of 0.14. A complete listing of crystallographic data, including a summary of the structure determination and tables of atom positions, thermal parameters, bond distances, and bond angles, is included in the Supporting Information.

Figure 5 depicts one molecule of **2**, which clearly shows that the pyrimidine ring of the L-keto ligand has been cleaved with excision of one carbon atom. Interestingly, the carbonyl group that had been exocyclic in the parent L-keto ligand has been rotated into an endocyclic position while the previously ring amide atom N21 now occupies an exocyclic position. In this position the oxygen atom O20 is able to participate in a

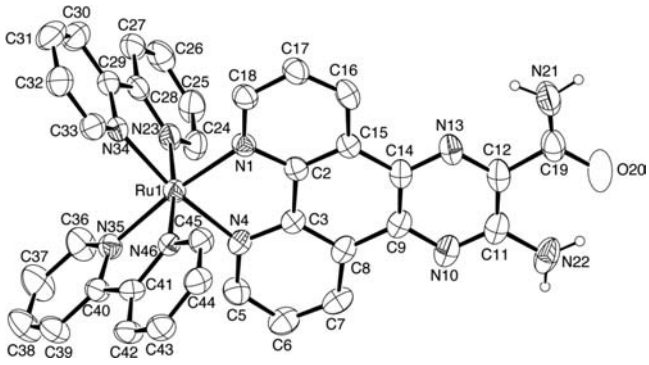

Figure 5. ORTEP drawing of Ru(L-aap) with 30% probability thermal ellipsoids shown.

stabilizing hydrogen bond interaction with the nearby proton on amine N22 (O20–N22 = 2.592 Å). The remaining structural features of **2** are unremarkable: all Ru–N bond distances fall within the range of 2.048(6)–2.065(5) Å, which are similar to both $[Ru(bpy)_2(L\text{-}Me_2allox)](PF_6)_2$[25] and $[Ru(bpy)_3]^{2+}$.[39] However, N–Ru–N bond angles for all chelating ligands, both the L-aap and the bpy ligands, have a large deviation with a bond angle range of 78.6(2)–97.1(2)°.

The asymmetric unit consists of two Ru-complex cations, four PF_6^- anions, one molecule each of chloroform and acetonitrile. Figure 6 provides several views of the packing interactions within the unit cell (Figure 6A), the asymmetric unit (Figure 6B), and between Ru complexes from adjacent cells (Figure 6C). Within the asymmetric unit, the two Ru complexes are oriented such that two bpy ligands are roughly coplanar (7.7 deg) with 3.6 Å separation, but are offset and do not exhibit significant π-stacking. The L-aap ligands between two Ru complexes of adjacent cells stack at 3.5 Å making an angle of 4.5° such that the bridgehead carbons between the phen and pyrazine rings are oriented over the pyrazine ring.

Infrared Spectroscopy. The most distinctive features observed in the FT-IR spectra of complexes **1** and **2** are the strong $\nu_{C=O}$ and $\nu_{C=N}$ stretching vibrations within the pteridyl-phenanthroline ligands. The carbonyl $\nu_{C=O}$ stretch in the L-keto ligand of **1** is observed at 1716 cm^{-1}, nearly identical to the $\nu_{C=O}$ frequency 1705 cm^{-1} in the uncoordinated ligand, whereas this mode in the ring-opened L-aap ligand in **2** occurs at 1683 cm^{-1}. This 33 cm^{-1} shift to lower energy is consistent with the X-ray structure placing the carbonyl endocyclic to hydrogen bond with the pyrazine amine group. Both **1** and the uncoordinated ligand have $\nu_{C=N}$ stretching modes at 1606 and 1607 cm^{-1}, respectively, but the absence of this mode in **2** may be due to the loss of the pyrimidine C=N group during the ring cleavage reaction. For Ru(L-amino), the $\nu_{C=N}$ stretch mode is seen at 1631 cm^{-1} and the ν_{N-H} bending mode at 1560 cm^{-1}. A broad peak at 1720 cm^{-1} represents the carbonyl stretches in Ru(L-allox).

NMR Spectroscopy. All complexes in this study were analyzed via ^1H, COSY, and NOESY NMR. The overlapping low field regions for phenanthroline and bipyridine protons cause complicated ^1H spectra, but assignments for these protons could be made by interpreting 2D COSY NMR experiments. Figure 7 shows ^1H NMR spectral assignments from COSY NMR for complexes Ru(L-keto) **1** and Ru(L-aap) **2** compared to the structurally related complexes Ru(L-allox) and Ru(L-amino) in d_6-DMSO. While the proton spectra of these four complexes share similar chemical shift patterns in the

dx.doi.org/10.1021/ic301219z | Inorg. Chem. 2012, 51, 12669–12681

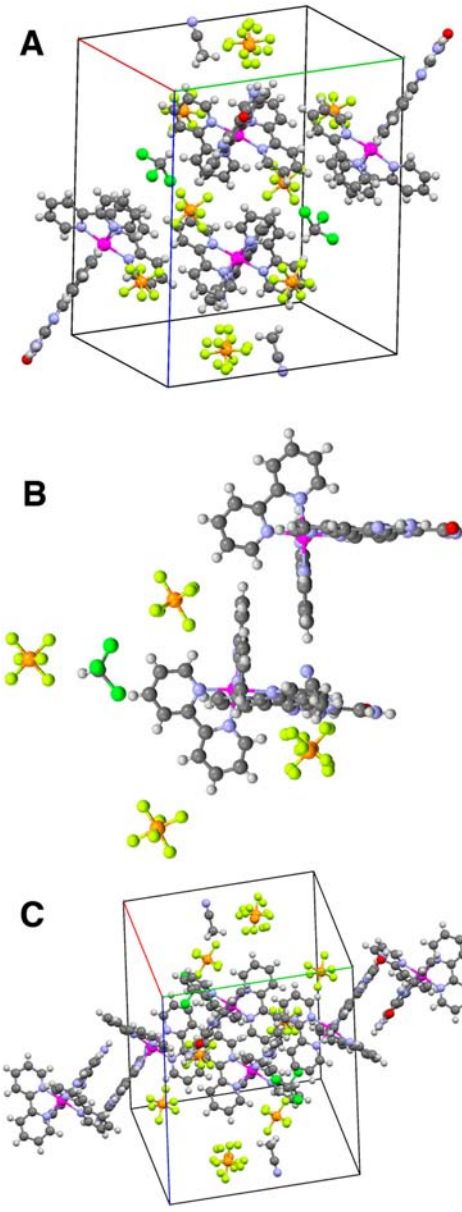

Figure 6. (A) Unit cell of $[Ru(bpy)_2(L\text{-}aap)](PF_6)_2$ **2** showing the packing of two molecules of **2**, one acetonitrile, one chloroform, three ordered and one disordered hexafluorophosphate molecules in each asymmetric unit, (B) the contents of the asymmetric unit showing the coplanar packing of two bpy ligands from each complex, (C) a second view of the unit cell plus two molecules of **2** in adjacent cells to illustrate the π stacking interaction of the L-aap ligands.

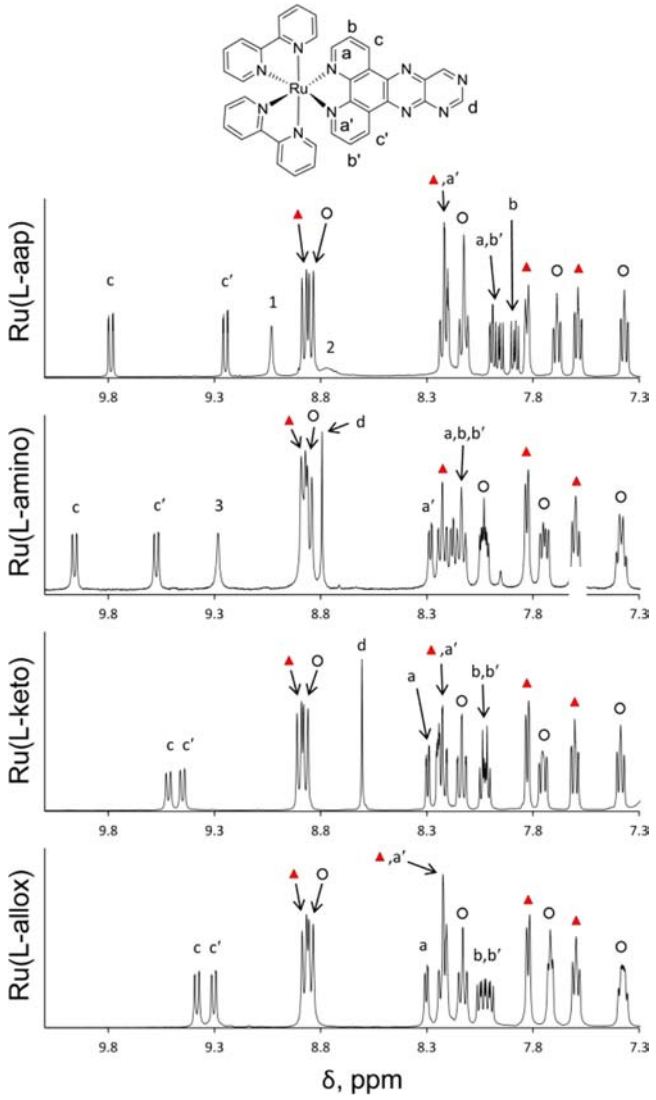

Figure 7. Comparison of the ^{1}H NMR spectra for Ru(L-keto) **1**, Ru(L-allox), Ru(L-aap) **2**, and Ru(L-amino) in d_6-DMSO at 28 °C with proton peak assignments determined by COSY experiments. Signals due to the two sets of inequivalent bpy protons are differentiated with open circles or red triangles. Labeled signals correspond to protons on special sites on the pteridinylphenanthroline system as illustrated in the drawing at top.

aromatic region, one notable difference is found in the region 8.5−10 ppm. Protons on the two bipyridine ligands (labeled with open circles and red triangles) and phenanthroline protons a, a′, b, and b′ appear at similar chemical shifts for Ru(L-keto) **1**, Ru(L-aap) **2**, Ru(L-amino), and Ru(L-allox) and exhibit little variation despite structural differences among the ligands. However, phenanthroline protons c and c′ are useful reporters of structural change among the four complexes.

Each of the four complexes **1**, **2**, Ru(L-allox), and Ru(L-amino) exhibit a pair of signals due to phenanthroline protons Hc and Hc′ between 9.0 and 10.0 ppm. The separation between the Hc and Hc′ resonances is distinctly larger (∼0.5 ppm) for Ru(L-amino) and Ru(L-aap) than is observed for Ru(L-keto) or Ru(L-allox) (∼0.1 ppm). This difference between the Hc and Hc′ resonances appears to correlate with the pyrimidine substitution where the larger separation occurs when an amino group is in the exocyclic position at C4 (numbering shown in Figure 3) and the smaller separation is produced by exocyclic carbonyl substituents. A likely reason for this variation in Hc, Hc′ chemical shifts is a through space interaction between the C4 substituent and the phenanthroline Hc. The adjacent amino group (N-Hc = 2.9 Å in Ru(L-amino) and 2.6 Å in **2**) is ∼1 Å closer than the carbonyl oxygen atom (O-Hc = 3.9 Å in Ru(L-allox) and **1**) and allows a stronger through-space interaction producing a more downfield-shifted phenanthroline Hc resonance. This observation corroborates the exocyclic amine orientation in **2** determined by X-ray crystallography and confirms that the amide conformation is the same in the solution and solid states.

dx.doi.org/10.1021/ic301219z | *Inorg. Chem.* 2012, 51, 12669−12681

The ^{1}H NMR spectrum of Ru(L-aap) **2** (top spectrum, Figure 7) shows only two of the four exchangeable amine protons at 9.0 (Figure 7, resonance 1) and 8.8 ppm (Figure 7, resonance 2), with integrations corresponding to one proton. The other two amine protons were observed by changing solvent to acetone-d_6 and obtaining spectra at lower temperature (7 °C) to slow the proton exchange rate (Supporting Information). NOESY experiments in acetone-d_6 at 7 °C allowed assignment of the two pairs exchangeable protons (H1a, H1b) and (H2a, H2b) to the amine and the amide (Supporting Information). On the basis of the greater expected acidity of the amide protons, the more downfield (H1a, H1b) pair is assigned to the amide protons, and the (H2a, H2b) pair is assigned to the amine protons.

Electronic Spectroscopy. The electronic absorption spectra obtained in aqueous 10 mM phosphate (pH 7) buffer for both **1** and **2** are compared with spectra of Ru(L-allox) and Ru(L-amino) in Figure 8. All four complexes exhibit absorptions in

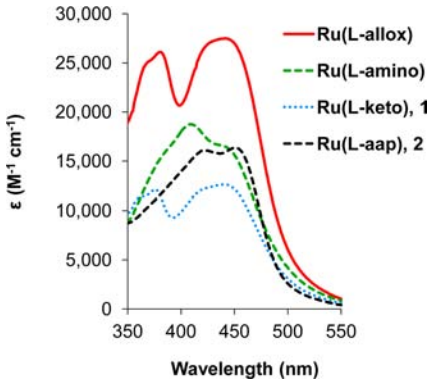

Figure 8. Electronic absorption spectra of **1**, **2**, Ru(L-allox), and Ru(L-amino). Solution are 30 μM in the Ru complex in 10 mM phosphate buffer at pH 7 and 25 °C.

the region between 350 and 500 nm with extinction coefficients of similar magnitude. The spectral assignments previously reported for Ru(L-allox) and Ru(L-amino)[25] were used to make assignments for the new compounds **1** and **2**. The electronic spectrum of **1** is nearly identical to that of Ru(L-allox), as might be expected given the similarity of their structures, and has the characteristic Ru→pteridinylphenanthroline MLCT band around 440 nm as well as overlapping $\pi-\pi^*$ transitions[40−42] of the pteridinylphenanthroline and bipyridine ligands between 350 and 380 nm where $\pi-\pi^*$ ligand transitions in **1** occur at slightly higher energies (~ 10 nm) than those of Ru(L-allox). In contrast, the spectra of both **2** and Ru(L-amino) show significant differences from the spectra of **1** and Ru(L-allox). The most distinctive difference concerns the $\pi-\pi^*$ transitions that are red-shifted in the spectrum of Ru(L-amino) to overlap part of the MLCT envelope between 350 and 400 nm, whereas these $\pi-\pi^*$ transitions are blue-shifted into the UV region in the spectrum of **2**. The MLCT region of **2** is more resolved than in any of the other complexes and is slightly red-shifted.

Cyclic Voltammetry. The redox behavior of the four complexes Ru(L-keto) **1**, Ru(L-aap) **2**, Ru(L-amino), and Ru(L-allox) was probed using CV. Voltammograms are shown in Figure 9, and electrochemical data is listed in Table 1 where potentials are referenced to ferrocenium/ferrocene (Fc+/Fc) used as an internal standard during experiments. Two solvents

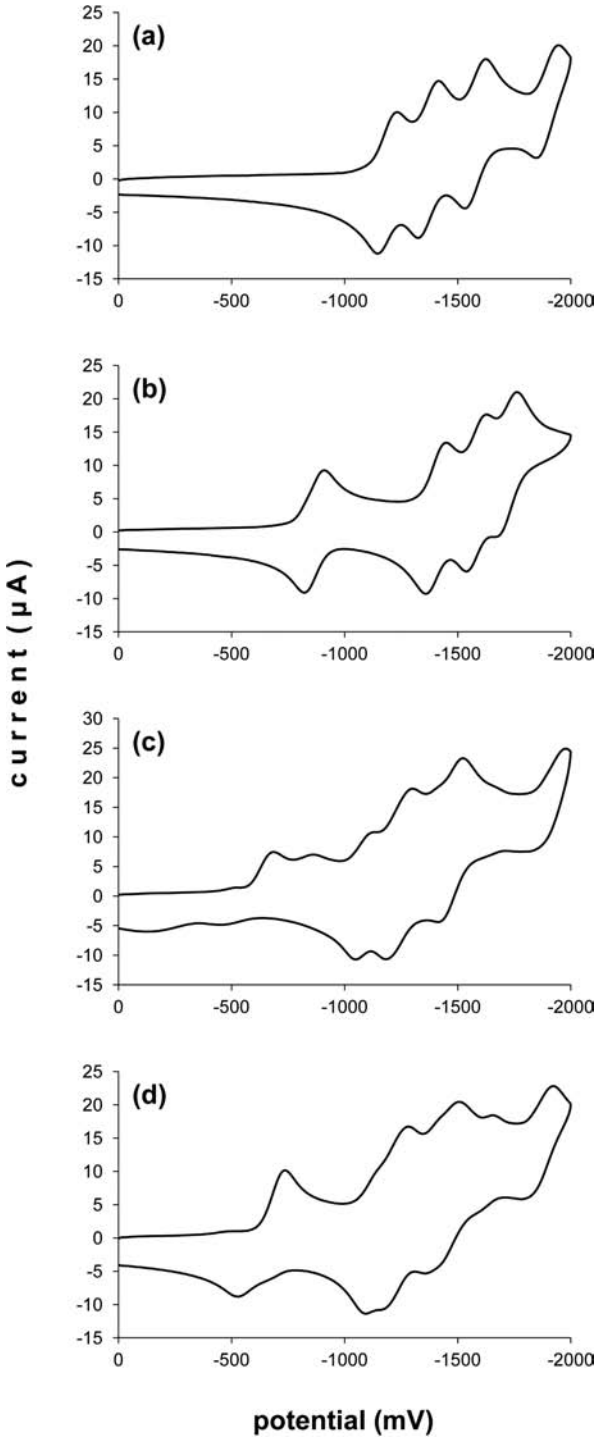

Figure 9. Cyclic voltammograms of (a) **2**, (b) Ru(L-amino), (c) **1**, and (d) Ru(L-allox), all at a scan rate of 100 mV/s in DMSO using a glassy carbon electrode.

and two working electrode materials were used in the CV experiments. Acetonitrile solutions and Pt electrodes allowed detection of the $Ru^{3+/2+}$ couple but produced poor signals from ligand-based processes in **1** and Ru(L-allox). Use of dimethylsulfoxide (DMSO) and changing to a glassy carbon working electrode improved the quality of ligands reductions; however, the potential window of DMSO did not allow detection of the $Ru^{3+/2+}$ couple.

Table 1. Electrochemical Data, Potentials Referenced to Ferrocene

complex	$E_{1/2}$ ($Ru^{3+/2+}$)[a]	$E_{1/2}$ (pter-phen)[b]	$E_{1/2}$ (bpy)[b]
Ru(L-aap) **2**	0.90	−1.60	−1.79, −1.99, −2.31
Ru(L-amino)	0.91	−1.22	−1.76, −1.94, −2.08
$[Ru(bpy)_2(dppz)]^{2+}$	0.92	−1.33	−1.77, −1.98, −2.22
$[Ru(bpy)_3]^{2+}$	0.87		−1.71, −1.89, −2.15
Ru(L-keto) **1**	0.94		−0.64[c], −0.96[c], −1.24[c], −1.41[c] −1.63, −1.79, −2.01, −2.42
Ru(L-allox)	0.91		−1.06[c], −1.28[c], −1.63[c], −1.77, −1.97, −2.17, −2.40

[a]Acetonitrile, Pt working electrode. [b]DMSO, glassy carbon working electrode. [c]Irreversible process.

The $Ru^{3+/2+}$ couple observed near +0.90 V is nearly invariant among the four complexes and only slightly more favorable than the observed metal oxidation in $[Ru(bpy)_3]^{2+}$ (+0.87 V). This indicates that the structural change on the pyrimidine ring, including cleavage of that ring in **2**, has negligible effect at the Ru atom. In contrast, the phenanthroline-derived ligand-based reductions are sensitive to changes in substitution and structure. In acetonitrile using a Pt working electrode, the two complexes bearing carbonyl groups, **1** and Ru(L-allox), exhibit poor electrochemical behavior (broad, irreversible peaks) typical of carbonyl-substituted pteridines. These reductions become more reversible in DMSO using a glassy carbon working electrode, as reported for electrochemical analysis of a related complex similar to Ru(L-allox).[43] The complexes with exocyclic amines, **2** and Ru(L-amino), exhibit well-resolved (chemically reversible) ligand-based redox processes in both solvent-electrode combinations. The redox processes between −1.22 and −1.60 V in **2** and Ru(L-amino) can be assigned to the phenanthroline-derived ligands and those processes between −1.71 and −2.31 V are assigned to the bpy ligands by comparison with $[Ru(bpy)_3]^{2+}$ and Ru-dppz (Table 1).[44,45] In contrast, the complexity of the ligand redox behavior of **1** and Ru(L-allox), where as many as 8 redox events are detected (Table 1), is not so easily interpreted.

DNA Studies. *DNA Intercalation.* The change in viscosity as molecules intercalate into DNA is viewed as one of the best indications of intercalative binding.[46] DNA titrated with increasing concentrations of an intercalating compound will exhibit increased viscosity because of DNA lengthening, and this phenomenon is commonly visualized as a plot of $(\eta/\eta_0)^{1/3}$ versus the ratio of intercalator to DNA.[21,46,47] The viscosity titrations for the new Ru complexes **1** and **2** were compared to the structurally related complexes Ru(L-allox) and Ru(L-amino)[25] in addition to the known metallointercalator Ru-dppz[48,49] in Figure 10. Positive slopes were observed for all five Ru complexes, providing strong evidence for DNA intercalation. The similarity in the viscosity plot slopes for **1** and **2** (black diamond and red triangle data, respectively) to the other three intercalating complexes suggests that all five complexes have comparable binding strength.[48,49] The strength of intercalative binding was measured by absorption titration as previously described for Ru(L-allox) and Ru(L-amino).[25] Figure 11 shows the titration curve and the fitted data for **2** while the same data for **1** is available in the Supporting

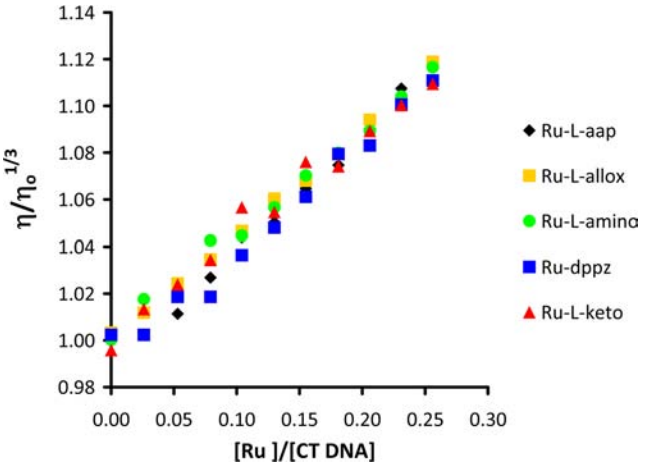

Figure 10. Viscosity titrations of CT DNA with **1**, **2**, Ru(L-allox), and Ru(L-amino) and positive control $[Ru(bpy)_2(dppz)]^{2+}$. Experimental conditions were 10 mM phosphate buffer pH 7, 50 mM NaCl.

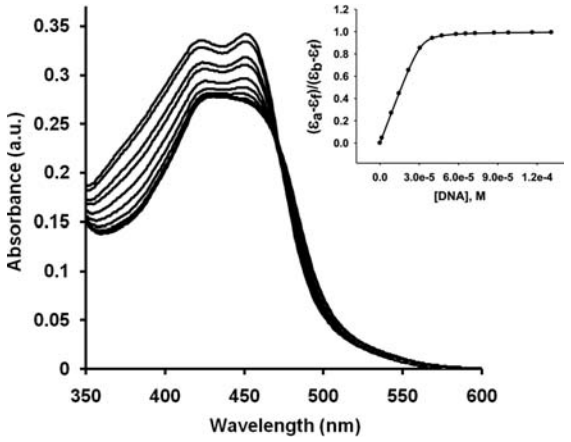

Figure 11. Absorption titration of **2** with increasing amounts of calf thymus DNA where the spectral series show a progression of decreasing intensity with increasing [DNA]/[Ru].

Information. Binding constant values, K_b, obtained from absorption titrations indicate that **2** binds more strongly ($K_b = 2.4 \pm 0.2 \times 10^6$, $s = 0.76$) than its parent complex **1** ($K_b = 5 \pm 1 \times 10^5$; $s = 0.96$). Binding constants for the structurally related complexes Ru(L-allox) and Ru(L-amino) are 4.7×10^5 and 2.6×10^6.[25] It is notable that higher K_b values are observed for Ru complexes with exocyclic amine groups on the pteridinyl-derived ligand as compared to exocyclic keto groups.

DNA Photocleavage. We have begun investigating the DNA photocleavage ability of the Ru-L-pteridine family of intercalators. The photocleavage of supercoiled pBR322 plasmid DNA by each compound was evaluated using agarose gel electrophoresis following the exposure of supercoiled pBR322 to 365 nm light in the presence of each Ru complex. Surprisingly, although the compounds are all good intercalators, they possess varying degrees of photocleavage ability. A comparison of the photocleavage abilities of **1**, **2**, Ru(L-allox), and Ru(L-amino) with the positive control Ru-dppz[50] is shown in Figure 12. No cleavage was observed when samples were incubated in the dark (data not shown). Under irradiation, the most efficient conversion of supercoiled to nicked DNA is afforded by the ring-cleaved complex **2** (lanes 3 and 4), and its photocleavage efficiency is significantly higher than Ru-dppz

dx.doi.org/10.1021/ic301219z | Inorg. Chem. 2012, 51, 12669−12681

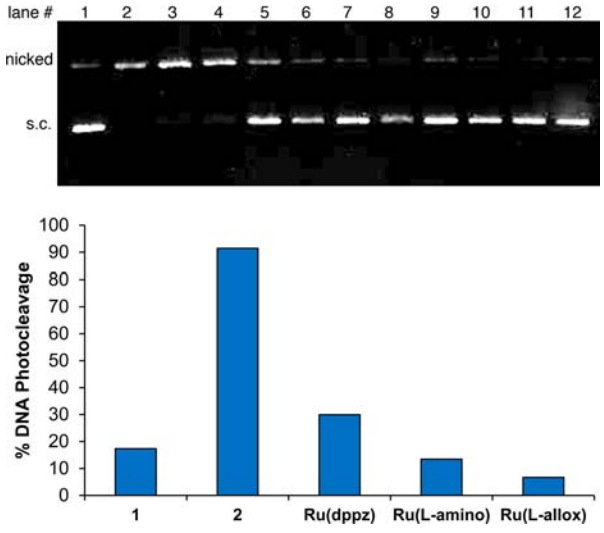

Figure 12. (top) Photocleavage of pBR322 plasmid DNA by Ru compounds with 120 min of UV exposure. Lane 1, supercoiled (s.c.) pBR322 alone; lane 2, nicked pBR322; lanes 3−12, alternating 16 and 160 μM of compounds: lanes 3−4, Ru(L-aap) **2**; lanes 5−6, Ru-dppz; lanes 7−8, Ru(L-amino); lanes 9−10, Ru(L-keto) **1**; lanes 11−12, Ru(L-allox). (bottom) Graphical depiction of the relative photocleavage abilities of the Ru complexes where % DNA Photocleavage = (intensity of nicked)/(intensity of nicked + supercoiled DNA) × 100% as calculated for each lane using ImageJ software to quantitate lane intensities.

(lanes 5 and 6). In contrast, generation of nicked DNA by the three pteridine complexes **1**, Ru(L-allox), and Ru(L-amino) (lanes 7−12) is negligible in comparison to the amount of relaxed DNA present in the supercoiled pBR322 plasmid (lane 1).

The effect of UV irradiation time and intercalator concentration for each ruthenium compound was varied to find optimal conditions, if any, for photocleavage. Complex **2** generated increasing amounts of nicked DNA with greater UV exposure time and with increasing concentrations of Ru compound up to 64 μM, beyond which photocleavage decreased (Figure 13). Samples of DNA and **2** incubated in the dark showed no cleavage.

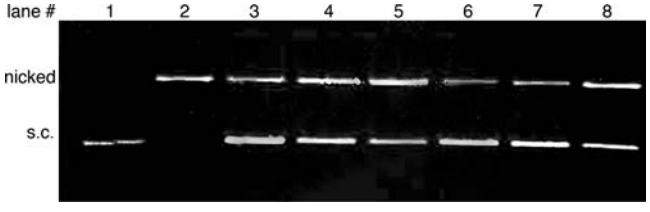

Figure 13. Photocleavage of pBR322 plasmid DNA by Ru(L-aap) **2**. Lane 1, supercoiled pBR322 alone (s.c.); lane 2, nicked pBR322; lanes 3−5, pBR322 treated with 1, 3, and 5 μM **2** respectively, lanes 6−8, pBR322 treated with 5 μM **2** with increasing length of UV exposure from 30−90 min.

We note our inability to reproduce the results of Gao and coworkers[50] who reported moderate photocleavage by Ru(L-allox). We could not detect any photocleavage of pBR322 by Ru(L-allox) under their reported conditions, nor in samples of Ru(L-allox) that were several months old. Figure 14 shows negligible photocleavage by Ru(L-allox) across a range of concentrations and irradiation times. Likewise, Ru(L-amino)

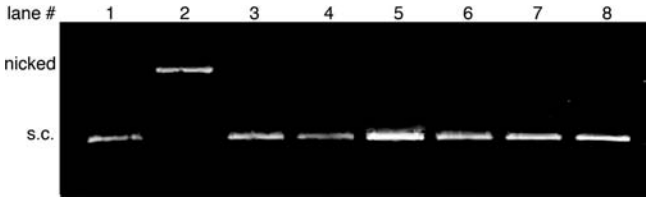

Figure 14. Photocleavage of pBR322 plasmid DNA by Ru(L-allox. Lane 1, supercoiled pBR322 alone (s.c.); lane 2, nicked pBR322; lanes 3−5, pBR322 treated with 16, 64, and 160 μM Ru(L-allox) respectively, lanes 6−8, pBR322 treated with 64 μM Ru(L-allox) with increasing length of UV exposure from 30−90 min.

exhibits no photocleavage under any concentration and increased UV exposure time.

Photocleavage studies using **1** gave inconsistent results in the amount of nicked DNA generated. Experiments done using fresh solutions of **1** prepared immediately prior to the photocleavage experiment yielded no photocleavage; however, experiments repeated a few days later using the same solution, showed moderate photocleavage. Ru-L-pteridine complexes are expected to be inert to ligand substitution at room temperature and all other Ru-L-pteridine complexes have demonstrated solution stability extending over periods of months (by ESI-MS). This inconsistency with **1** prompted us to investigate its stability when dissolved in the Tris-HCl buffer used for photocleavage experiments using ESI-MS. A series of 400 μM solutions of **1** in buffer (50 mM Tris-HCl, pH 7.2, with 18 mM NaCl) were made over a period of 15 days. These solutions of varying age were then analyzed by ESI-MS in concert with measuring their DNA photocleavage ability. It was determined by ESI-MS that **1** undergoes two reactions in solution at room temperature. First, water adds across the N1−C2 bond to make a hydrated Ru(L-keto) species and second, the pyrimidine ring cleaves to produce **2** (Figure 15). The ring-cleaved complex **2** is a highly efficient photocleaving agent, and its presence, even in small amounts, can account for the observation of increased photocleavage with old solutions of **1**. The time scale of **1** degradation into **2** is shown in Figure 16 where after a week ∼7% of **1** has undergone conversion to **2**, and after 2 weeks, the abundance of **2** is nearly 20%. The formation of the hydrated **1** reaches 20% after 2 days and then remains within the range of 20−30% over the course of the degradation study. As expected, within this series of samples the amount of photocleavage increased in concert with the amount of decomposition of **1** forming **2** measured by ESI-MS.

To evaluate whether the mechanism of plasmid DNA photocleavage by Ru(L-aap) **2** involved reactive oxygen species (ROS), photocleavage experiments were carried out in the presence of various radical scavengers as well as under anaerobic conditions (Figure 17). Plasmid photocleavage was completely inhibited under anaerobic conditions (lane 6) and partially inhibited in the presence of the singlet oxygen inhibitor sodium azide (lane 5).[52−54] Dimethylsulfoxide (DMSO), a hydroxyl radical scavenger,[55] had minimal effect on the photocleavage damage effected by complex **2** (lane 3). The enzyme superoxide dismutase (SOD), an inhibitor of superoxide, seems to increase, not inhibit, photocleavage as shown by the increased intensity of the nicked band in lane 4, which has been observed previously.[50]

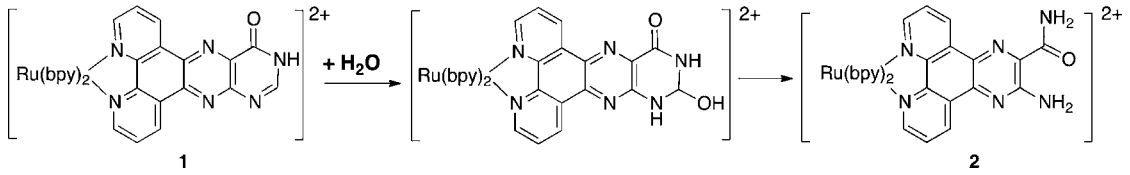

Figure 15. Degradation of **1** in buffer at pH 7.2 by hydration followed by ring cleavage to form **2**.

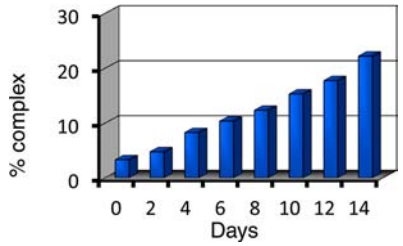

Figure 16. Percent abundance of Ru(L-aap) **2** formed over time (in days) from degradation of Ru(L-keto) **1** dissolved in 50 mM Tris-HCl (pH 7.2) with 18 mM NaCl as monitored by ESI-MS. The percent abundance of **2** is estimated by dividing the intensity of m/z signal at 352 for **2** by the sum of the signal intensities of all Ru species observed.

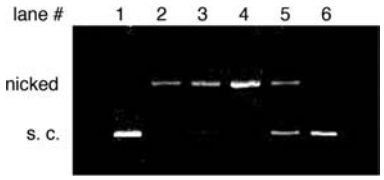

Figure 17. Photocleavage of pBR322 plasmid DNA by Ru(L-aap) **2** in the presence of various ROS inhibitors. Lane 1, supercoiled pBR322 alone; lane 2, pBR322 treated with **2**; lane 3, pBR322 treated with **2** and 100 mM DMSO, lane 4, pBR322 treated with **2** and 5 μg of SOD, lane 5, pBR322 treated with **2** and 2 mM NaN_3, lane 6, pBR322 treated with **2** anaerobic under N_2.

DISCUSSION

We have been exploring the N-heterocyclic pteridine system as a conjugated planar extension of 1,10-phenanthroline for synthesis of new Ru(II) polypyridyl complexes used in DNA studies. Previously we reported our initial results from this project where a series of Ru-pteridinyl-phenanthroline complexes were prepared with a variety of substitutions on the terminal pyrimidine ring of the pteridine system. The pteridine substitutions were chosen to include structures that mimic the H-bonding patterns of nucleic acids for the purpose of probing whether these might affect the Ru complex binding to DNA. We reported that all of the Ru-pteridinyl-phenanthroline complexes bound to DNA by intercalation with binding constants within an order of magnitude of that for Ru-dppz. The goal of the work reported here was the study of a new, monocarbonyl member of the pteridine family, Ru(L-keto) **1**. During synthesis of **1** we discovered that a second Ru complex, Ru(L-aap) **2**, was produced at higher reaction temperatures. This high temperature product **2** results from loss of C2 in the pyrimidine ring, and the remnants of the pyrimidine ring form amide and amine groups on the 2,3 positions of the pyrazine ring. Exploration of the conditions promoting formation of **2** support a mechanism proceeding through nucleophilic attack of hydroxide followed by elimination of C2 as formate. This is consistent with prior studies of pyrimidine ring cleavage in pteridines and related N-heterocycles.[33−39] The X-ray structure of **2** revealed that the remaining amide group is rotated placing the amine group exocyclic and the amide carbonyl in a position stabilized by both H-bonding to the 2-amino group and formation of a six-membered ring.

Both of the new complexes **1** and **2** are good intercalators of CT DNA based on viscosity and absorption titration experiments. The binding constant of **1** is nearly identical to that of its close structural relative Ru(L-allox) while the K_b measured for **2** indicates it binds as strongly as Ru-dppz.[25] Despite the similar intercalation ability of the five Ru complexes **1**, **2**, Ru(L-allox), Ru(L-amino), and Ru-dppz, not all of them photocleave plasmid DNA when irradiated by UV light. We find that the ring-cleaved complex Ru(L-aap) **2** photocleaves DNA significantly more effectively than Ru-dppz, but neither the parent pteridine complex Ru(L-keto) **1** nor the structurally related complexes Ru(L-allox) and Ru(L-amino) exhibit *any* photogenerated nicked DNA under a range of conditions. The lack of observed photocleavage by Ru(L-allox) is particularly noteworthy since it had been reported to induce moderate photocleavage in pBR322 under the same conditions employed in our study.[50]

During the photocleavage experiments, we found that **1** has limited stability in buffer at ambient temperature where it undergoes two reactions on the pteridinyl-phenanthroline ligand: addition of water across a C=N bond followed by pyrimidine ring cleavage to produce complex **2**. The formation of the powerful photocleaver **2** from degradation of **1** in buffer initially led to misleading results of photocleavage activity of **1**. In contrast, this reactivity was not observed either in Ru(L-amino) or Ru(L-allox). Regardless, this reaction is significant as an example of how Ru complexes under typical conditions used in DNA studies may undergo reactions leading to more active DNA cleavers. It also suggests that in situ reactivity of Ru complexes with DNA should be considered.

Of the two predominant mechanisms for oxidative damage to DNA mediated by Ru polypyridyl complexes, direct oxidation of DNA bases and oxidation by singlet oxygen ($^1O_2$),[5,56−58] complex **2** appears to photocleave DNA through a singlet oxygen mechanism. The majority of studies on ruthenium-induced DNA cleavage have identified singlet oxygen as the reactive oxygen species (ROS) that damages the DNA.[56,57,59] In this mechanism, polypyridyl complexes like $[Ru(bpy)_2dppz]^{2+}$ are good photosensitizers of molecular oxygen to produce a high energy singlet state of dioxygen. Photocleavage experiments gave results consistent with the singlet oxygen mechanism: no photocleavage by **2** occurs under anaerobic conditions and only azide, a singlet oxygen inhibitor, has a negative effect on the extent of its photocleavage of pBR322 plasmid DNA.

The characteristics of Ru complexes required for DNA photocleavage are currently under investigation in our laboratories. Intercalative ability is not sufficient in Ru complexes to produce photocleavage behavior, as shown by the results presented here. Ru(L-allox) intercalates nearly as

dx.doi.org/10.1021/ic301219z | Inorg. Chem. 2012, 51, 12669−12681

well as Ru-dppz, and the electronic spectra of these two complexes are almost superimposable, but Ru(L-allox) exhibits no photocleavage under the same conditions where Ru-dppz causes significant DNA photoinduced damage. A comparison of the relative molar absorptivities at 365 nm (Figure 8) and the photocleavage results (Figure 12) indicates there is no direct correlation between the absorptivity of a complex at the irradiation wavelength and its ability to damage DNA by photocleavage. In contrast, the ring-cleaved complex **2** intercalates DNA with a binding strength identical to Ru-dppz but produces much more extensive photocleavage damage. One unique feature of **2** that may correlate with its superior photocleavage activity is the more negative first reduction potential, attributed to the L-aap ligand, as compared to the reduction potentials observed for the other pteridinyl-phenanthroline ligands (Table 1) and for the dppz ligand reduction. The more negative reduction potential in **2** may indicate a higher energy photoexcited state that generates a more effective dioxygen sensitizer. The significance of this observation may be put in context through work of Turro et al. who correlated the presence of long-lived low lying triplet states in Ru-polpyridyls with high quantum yields of $^1O_2$.[60,61] A possibility not pursued in this work is that UV irradiation of **2** may likewise generate a long-lived $^3\pi\rightarrow\pi^*$ excited state that is responsible for high levels of $^1O_2$ production.

Currently experiments are directed at quantifying the singlet oxygen produced by **2** and all the $[Ru(bpy)_2(pteridinyl-phenanthroline)]^{2+}$ complexes in this family.

CONCLUSION

We have presented our investigation of two ruthenium(II) pteridinyl-phenanthroline complexes, $[Ru(bpy)_2(L\text{-keto})](PF_6)_2$ **1** and $[Ru(bpy)_2(L\text{-aap})](PF_6)_2$ **2**, where chelation of L-keto to Ru(II) in **1** appears to facilitate a pyrimidine ring cleavage producing **2**. While both **1** and **2** are good intercalators of calf thymus DNA, only the ring-cleaved complex **2** exhibits an unusually high degree of pBR322 plasmid photocleavage, a behavior that is in sharp contrast to the inability of other pteridinyl-phenanthroline complexes to effect any photocleavage of plasmid DNA. We note that while **1** has no inherent photocleavage ability, its instability in buffer where it degrades to **2** is an example of how in situ reactions of potential photocleavage agents can present problems in accurately measuring the degree of photocleavage. No photocleavage by **2** occurs under anaerobic conditions and the use of the singlet oxygen scavenger azide suppresses photocleavage. These results support a Ru(II) photogenerated singlet oxygen mechanism for the DNA damage caused by **2**.

ASSOCIATED CONTENT

Supporting Information

Listings of CIF file, NMR spectra, cyclic voltammagrams, electronic absorption, and DNA titrations and binding data. This material is available free of charge via the Internet at http://pubs.acs.org.

AUTHOR INFORMATION

Corresponding Author

*E-mail: sburgmay@brynmawr.edu.

Notes

The authors declare no competing financial interest.

ABBREVIATIONS

L-keto = 4-keto-pteridino[6,7-*f*]phenanthroline
L-aap = 2,-amino-3-amidopyrazino[5,6-*f*]phenanthroline
L-allox = 2,4-diketo-pteridino[6,7-*f*]phenanthroline
L-amino = 4-amino-pteridino[6,7-*f*]phenanthroline
L-pteridine = any of the above four ligands
$Ru(L\text{-aap}) = [Ru(bpy)_2(L\text{-aap})](PF_6)_2$
$Ru(L\text{-allox}) = [Ru(bpy)_2(L\text{-allox})](PF_6)_2$
$Ru(L\text{-keto}) = [Ru(bpy)_2(L\text{-keto})](PF_6)_2$
$Ru\text{-dppz} = [Ru(bpy)_2(dppz)]^{2+}$
EtBr = ethidium bromide
CT DNA = calf thymus DNA

REFERENCES

(1) *DNA and RNA Binders: from Small Molecules to Drugs*; Demeunynck, M., Bailly, C., Wilson, W. D., Eds.; Wiley-VCH: Weinheim, Germany, 2003; Vol. *1*; p 146.
(2) (a) Farrell, N. *Coord. Chem. Rev.* **2002**, *232*, 1−4. (b) *Metallotherapeutic Drugs and Metal-Based Diagnostic Agents: the Use of Metals in Medicine*; Gielen, M., Tiekink, E. R. T., Eds.; Wiley: London, U.K., 2005; p 359.
(3) Erkkila, K. E.; Odom, D. T.; Barton, J. K. *Chem. Rev.* **1999**, *99*, 2777−2796.
(4) Sigman, D. S.; Mazumder, A.; Perrin, D. M. *Chem. Rev.* **1993**, *93*, 2295−2316.
(5) Armitage, B. *Chem. Rev.* **1998**, *98*, 1171−1200.
(6) Boerner, L. J. K.; Zaleski, J. M. *Curr. Opin. Chem. Biol.* **2005**, *9*, 135−144.
(7) Kelley, S. O.; Jackson, N. M.; Hill, M. G.; Barton, J. K. *Angew. Chem., Int. Ed.* **1999**, *38*, 941−945.
(8) Kelley, S. O.; Holmlin, R. E.; Stemp, E. D. A.; Barton, J. K. *J. Am. Chem. Soc.* **1997**, *119*, 9861−9870.
(9) Fu, P. K. L.; Bradley, P. M.; Turro, C. *Inorg. Chem.* **2003**, *42*, 878−884.
(10) Jung, Y. W.; Lippard, S. J. *Chem. Rev.* **2007**, *107*, 1387−1407.
(11) Genereux, J. C.; Boal, A. K.; Barton, J. K. *J. Am. Chem. Soc.* **2010**, *132*, 891−905.
(12) Elias, B.; Kirsch-DeMesmaeker, A. *Coord. Chem. Rev.* **2006**, *250*, 1627−1641.
(13) Friedman, A. E.; Chambron, J. C.; Sauvage, J. P.; Turro, N. J.; Barton, J. K. *J. Am. Chem. Soc.* **1990**, *112*, 4960−4962.
(14) Jenkins, Y.; Friedman, A. E.; Turro, N. J.; Barton, J. K. *Biochemistry.* **1992**, *31*, 10809−10816.
(15) Holmlin, R. E.; Stemp, E. D. A.; Barton, J. K. *Inorg. Chem.* **1998**, *37*, 29−34.
(16) Elias, B.; Creely, C.; Doorley, G. W.; Feeney, M. M.; Moucheron, C.; Kirsch-DeMesmaeker, A.; Dyer, J.; Grills, D. C.; George, M. W.; Matousek, P.; Parker, A. W.; Towrie, M.; Kelly, J. M. *Chem.—Eur. J.* **2008**, *14*, 369−375.
(17) Chouai, A.; Wicke, S. E.; Turro, C.; Bacsa, J.; Dunbar, K. R.; Wang, D.; Thummel, R. P. *Inorg. Chem.* **2005**, *44*, 5996−6003.
(18) Mongelli, M. T.; Heinecke, J.; Mayfield, S.; Okyere, B.; Winkel, B. S. J.; Brewer, K. J. *J. Inorg. Biochem.* **2006**, *100*, 1983−1987.
(19) Liu, X. W.; Li, J.; Li, H.; Zheng, K. C.; Chao, H.; Ji, L. N. *J. Inorg. Biochem.* **2005**, *99*, 2372−2380.
(20) Maheswari, P.; Palaniandavar, M. *J. Inorg. Biochem.* **2004**, *98*, 219−230.
(21) Ambroise, A.; Maiya, B. G. *Inorg. Chem.* **2000**, *39*, 4256−4263.
(22) Kumar, K. A.; Reddy, K. L.; Satyanarayana, S. *Transition Met. Chem.* **2010**, *35*, 713−720.
(23) Tan, L. F.; Chao, H.; Zhou, Y. F.; Ji, L. N. *Polyhedron* **2007**, *26*, 3029−3036.
(24) Hall, J. P.; O'Sullivan, K. O.; Naseer, A.; Smith, J. A.; Kelly, J. M.; Cardin, C. J. *Proc. Natl. Acad. Sci. U.S.A.* **2011**, *108*, 17610−17614.
(25) Dalton, S. R.; Glazier, S.; Leung, B.; Win, S.; Megatulski, C.; Burgmayer, S. J. N. *J. Biol. Inorg. Chem.* **2008**, *13*, 1133−1148.

(26) Yamada, M.; Tanaka, Y.; Yoshimoto, Y.; Kuroda, S.; Shimao, I. *Bull. Chem. Soc. Jpn.* **1992**, *65*, 1006−1011.
(27) Sullivan, B. P.; Salmon, D. J.; Meyer, T. J. *Inorg. Chem.* **1978**, *17*, 3334−3341.
(28) Sheldrick, G. M. *SADABS*; University of Göttingen: Göttingen, Germany, 2007.
(29) Sheldrick, G. M. *Acta Crystallogr., Sect. A* **2008**, *64*, 112−122.
(30) Reichmann, M. E.; Rice, S. A.; Thomas, C. A.; Doty, P. *J. Am. Chem. Soc.* **1954**, *76*, 3047−3053.
(31) Cohen, G.; Eisenberg, H. *Biopolymers* **1968**, *6*, 1077−1100.
(32) Carter, M. T.; Rodriquez, M.; Bard, A. J. *J. Am. Chem. Soc.* **1989**, *111*, 8901−8911.
(33) Baker, B. R.; Joseph, J. P. *J. Am. Chem. Soc.* **1955**, *77*, 15−18.
(34) Fujii, T.; Saito, T.; Terahara, N. *Chem. Pharm. Bull.* **1986**, *34*, 1094−1107.
(35) Itaya, T.; Ito, N.; Kanai, T.; Fujii, T. *Chem. Pharm. Bull.* **1997**, *45*, 832−841.
(36) Montgomery, J. A.; Thomas, H. J. *J. Med. Chem.* **1972**, *15*, 182−187.
(37) Montgomery, J. A.; Laseter, A. G.; Shortnacy, A. T.; Clayton, S. J.; Thomas, H. J. *J. Med. Chem.* **1975**, *18*, 564−567.
(38) Curran, W. V.; Angier, R. B. *J. Org. Chem.* **1961**, *26*, 2364−2368.
(39) Tsou, K. C.; Yip, K. F.; Miller, E. E.; Lo, K. W. *Nucleic Acids Res.* **1974**, *1*, 531−547.
(40) Otsuka, T.; Sekine, A.; Fujigasaki, N.; Ohashi, Y.; Kaizu, Y. *Inorg. Chem.* **2001**, *40*, 3406−3412.
(41) Fantacci, S.; De Angelis, F.; Sgamellotti, A.; Re, N. *Chem. Phys. Lett.* **2004**, *396*, 43−48.
(42) Xu, L. C.; Li, J.; Shen, Y.; Zheng, K. C.; Ji, L. N. *J. Phys. Chem. A* **2007**, *111*, 273−280.
(43) Olaprath, W.; McGuire, M. E. *Inorg. Chim. Acta* **2012**, *383*, 312−315.
(44) Delaney, S.; Pascaly, M.; Bhattacharya, P. K.; Han, K.; Barton, J. K. *Inorg. Chem.* **2002**, *41*, 1966−1974.
(45) Fees, J.; Ketterle, M.; Klein, A.; Fiedler, J.; Kaim, W. *J. Chem. Soc., Dalton Trans.* **1999**, *15*, 2595−2599.
(46) Suh, D.; Chaires, J. B. *Bioorg. Med. Chem.* **1995**, *3*, 723−728.
(47) Vaidyanathan, V. G.; Nair, B. U. *J. Inorg. Biochem.* **2003**, *95*, 334−342.
(48) Dupureur, C. N.; Barton, J. K. *Inorg. Chem.* **1997**, *36*, 33−43.
(49) Tuite, E.; Lincoln, P.; Norden, B. *J. Am. Chem. Soc.* **1997**, *119*, 239−240.
(50) Sun, Y.; Collins, S. N.; Joyce, L. E.; Turro, C. *Inorg. Chem.* **2010**, *49*, 4257−4262.
(51) Gao, F.; Chao, H.; Zhou, F.; Yuan, Y. X.; Peng, B.; Ji, L. N. *J. Inorg. Biochem.* **2006**, *100*, 1487−1494.
(52) Yu, H. J.; Huang, S. M.; Li, L. Y.; Jia, H. N.; Chao, H.; Mao, Z. W.; Liu, J. Z.; Ji, L. N. *J. Inorg. Biochem.* **2009**, *103*, 881−890.
(53) Schweitzer, C.; Schmidt, R. *Chem. Rev.* **2003**, *103*, 1685−1757.
(54) Harbour, J. R.; Issler, S. L. *J. Am. Chem. Soc.* **1982**, *104*, 903−905.
(55) Lesko, S. A.; Lorentzen, R. J.; Ts'o, P. O. P. *Biochemistry.* **1980**, *19*, 3023−3028.
(56) Mei, H. Y.; Barton, J. K. *Proc. Natl. Acad. Sci.* **1988**, *85*, 1339−1343.
(57) Hergueta-Bravo, A.; Jiménez-Hernández, M. E.; Montero, F.; Oliveros, E.; Orellana, G. *J. Phys. Chem. B.* **2002**, *106*, 4010−4017.
(58) Deshpande, M. S.; Kumbhar, A. A.; Kumbhar, A. S.; Kumbhakar, M.; Pal, H.; Sonawane, U. B.; Joshi, R. R. *Bioconjugate Chem.* **2009**, *20*, 447−459.
(59) Kalyanasundaram, K. *Coord. Chem. Rev.* **1982**, *46*, 159−244.
(60) Sun, Y.; Joyce, L. E.; Dickson, N. M.; Turro, C. *Chem. Commun.* **2010**, *46*, 2426−2428.
(61) Sun, Y.; Ojaimi, M. E.; Hammitt, R.; Thummel, R. P.; Turro, C. *J. Phys. Chem. B* **2010**, *114*, 14664−14670.